Progress In Electromagnetics Research Letters, Vol. 103, 15–23, 2022

2D Hybrid Magnetic Model Calculation in Axisymmetric Device

Abdi Ammar*

Abstract—This paper proposes a 2D semi-analytical electromagnetic model to compute the magnetic field and eddy current generated by a variable current density along a conducting billet of induction heater. The developed model is based on the combination of the discretization method and the Biot-Savart theory. Firstly, the analytical solutions of the vector potential and magnetic field are calculated in all elements discretized cylindrical geometry using the law of Biot-Savart. Then, the total field is determined by the contribution of the superposition of each element of the discretized geometry. The eddy currents are computed using the Ampere law, and it also allows us to determine the exact resulting heating power density, which is the heat source of the thermal problem. The results obtained are in agreement with those obtained using finite element method. Therefore, the developed magnetic model presents a fast and accurate tool for the design of induction heating devices.

1. INTRODUCTION

Induction heating is widely used in many industrial applications, surface heat, treatment and core heating [1, 2]. The well-known principle is based on the fact that any stationary conductor placed in a variable magnetic field is flowed by eddy currents creating Joule losses [3–5]. Another induction heating process is to move the conductive plate in a static magnetic field [2, 5].

The study of induction heating devices in general requires multi-physics modeling, which involves coupled magneto-thermal phenomena [6]. Knowledge of the electromagnetic field in all the electromagnetic devices allows accessing the calculation of the operating performance of these devices [7–9]. For this purpose, three types of methods have already been applied in the literature, numerical, analytical, or hybrid methods [10–20]. The choice of method depends on the nature and geometry of the problem. In an axisymmetric system, two-dimensional induction field can be perfectly described by means of the tangential component of the vector potential; this is not the case for non-axisymmetric systems.

This work proposes a new semi-analytical field calculation model based on the synergy between numerical method and the method of elliptic integrals, and this technique is applicable to all systems with axis of symmetry therefore two-dimensional.

First, the geometry is discretized into meshes; the magnetic potential is calculated from the Biot-Savart equation thanks to the elliptic integrals method in all elements. The total field is determined by superposing the contribution of each element of a discretized geometry. The total field is then used to calculate the induced currents in the workpiece as well as the heat power density, which represents the heat source.

Finally, the obtained results are validated and compared in those obtained using finite element method.

Received 2 January 2022, Accepted 7 February 2022, Scheduled 18 February 2022

* Corresponding author: Abdi Ammar (aabdi@usthb.dz).

The author is with the Electrical and Industrial Systems Laboratory, Faculty of Electronics and Computer Science (LSEI), University of Science and Technology Houari Boumediene, Algiers 16111, Algeria.

2. MAGNETIC SEMI-ANALYTICAL MODEL

2.1. Geometry Description and Assumptions

We consider a coil of radius r_c powered by a current density J whose general shape is shown in Fig. 1, knowing that the system has a symmetry of rotation. The problem is two-dimensional, so we take the resolution in a half-plane device.

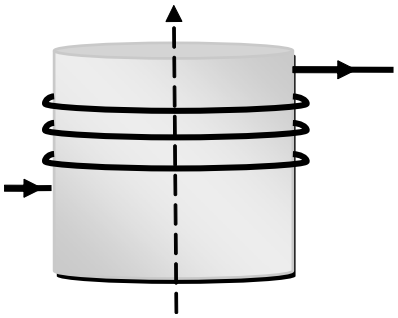

Figure 1. Geometry description of the induction heater.

The main geometrical parameters and structure in the (r, z) plane, physical proprieties, and geometrical dimensions of the studied induction heater are shown respectively in Fig. 2 and Table 1.

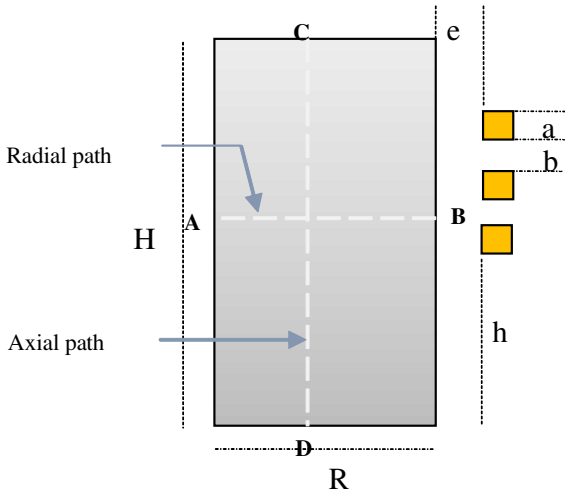

Figure 2. 2D geometric simplified model.

2.2. 2D Magnetic Analytical Model

In this study, the electromagnetic problem is formulated in 2D with magnetic vector potential $\vec{A}$. Based on the integral of Biot-Savart formula, the magnetic vector potential $\vec{A}$ at any point P in coordinates (r, z) is given by the following equation [2]:

$$A(p) = \frac{\mu_o}{4\pi} \int \frac{J(P_o)}{|P - P_o|} dV_o \tag{1}$$

Due to the symmetry to oz (Fig. 2), $\vec{A}$ is only a function of r and z, from which the following expression:

$$A(r, z) = \frac{\mu_o}{2\pi} J(r_c, z_c) \sqrt{\frac{r_c}{r}} G(k) \tag{2}$$

With:

$$G(k) = \frac{\left(2-k^2\right)E_1(k) - E_2(k)}{k} \tag{3}$$

$$E_1(k) = \int_0^{\frac{\pi}{2}} \frac{d\varphi}{\sqrt{1-k^2\sin^2(\varphi)}} \tag{4}$$

$$E_2(k) = \int_0^{\frac{\pi}{2}} \sqrt{1-k^2\sin^2(\varphi)}d\varphi \tag{5}$$

$$k = \sqrt{\frac{4r_c r}{(r_c+r)^2+(z-z_c)^2}} \tag{6}$$

$E_1(k)$, $E_2(k)$ are incomplete elliptic integrals of Legendre of the first and second kinds, respectively. Using the expansion of the Taylor series, the expressions of Legendre's elliptical integrals become:

$$E_1(k) = \frac{\pi}{2}\left[1+2\left(\frac{k^2}{8}\right)+9\left(\frac{k^2}{8}\right)^2+\ldots\right] \tag{7}$$

$$E_2(k) = \frac{\pi}{2}\left[1+2\left(\frac{k^2}{8}\right)-9\left(\frac{k^2}{8}\right)^2+\ldots\right] \tag{8}$$

These integrals are given in polynomial form, by the following expressions

$$E_1(k) = 1.3862944 + 0.1119723M_1 + 0.0725296M_2 + (0.5 + 0.1213478M_1 + 0.0288729M_2)C \tag{9}$$

$$E_2(k)\,1 + 0.4630151M_1 + 0.1077812M_2 + (0.245272M_1 + 0.0412496\,M_2)C \tag{10}$$

With:

$$M_1 = 1-k^2$$
$$M_2 = M_1^2$$
$$C = -\log(M_1)$$

2.3. Expressions of Electrical and Magnetic Quantities

The magnetic vector potential at each point in the study area depends on all the currents existing in each region. In this case, taking into account the induced currents, the calculation of the current density is given by:

$$J(r,z) = -jw\sigma(r,z)A(r,z) \tag{11}$$

The value of the magnetic vector potential is given after summing all the effects of the current loops and will therefore:

$$A(r,z) = \frac{\mu_o}{2\pi}\sum\nolimits_{i=1}^{n}\sum\nolimits_{j=1}^{m}\sqrt{\frac{r_c}{r}}J(i,j)\,SG(k_i) \tag{12}$$

To calculate the total potential, we used an iterative method which resulted in the flowchart of Fig. 3. Knowing the value of the vector potential in all the points of field of study, we can thus calculate the electromagnetic quantities given as follows:

$$Br(r,z) = \frac{\mu_o}{8\pi}\frac{z-z_c}{r}I(r_c z_c)\frac{k}{\sqrt{rr_c}}\left[\frac{2-k^2}{1-k^2}E_2(k) - 2E_1(k)\right] \tag{13}$$

$$Bz(r,z) = \frac{\mu_o}{8\pi}I(r_c,z_c)\frac{k}{\sqrt{rr_c}}\left[\frac{2-\left(1+\frac{r_c}{r}\right)}{1-k^2}E_2(k) - 2E_1(k)\right] \tag{14}$$

The expressions of electric field and the density of induced current are given respectively by:

$$\vec{E} = -\frac{\partial\vec{A}}{\partial t}, \quad \vec{J}_{ind} = \sigma\vec{E} \tag{15}$$

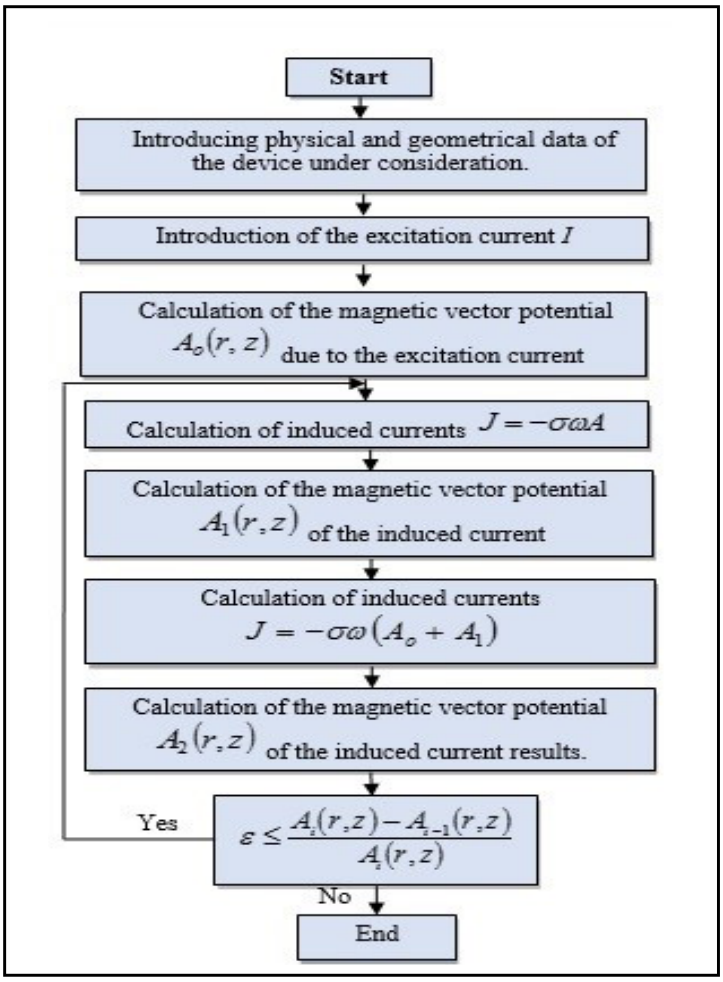

Figure 3. Flowchart field computing.

The average power dissipated by Joule effect is given by:

$$Q = \frac{1}{2\sigma} JJ^*, \quad \vec{J}_{ind} = \sigma\vec{E} \tag{16}$$

This allows us to write the average power density as a module:

$$Q = \frac{1}{2}\sigma w^2 A^2 \tag{17}$$

The total losses in the conductive part are the sum of the individual losses of mesh N.

$$P_T(t) = \sum_{i=1}^{N} P_i(t) \tag{18}$$

3. RESULTS AND VALIDATION

3.1. Semi-Analytical Electromagnetic Model Application

We compare in the following section some results of the electromagnetic problem, obtained by the semi-analytical model developed with those obtained by the 2D finite elements model. The results are obtained using $f = 50\,\text{Hz}$. The study concerns the induction heating device shown in Fig. 1. For the topology, all the dimensions and properties of the materials are found in Table 1.

Table 1. Physical and geometrical parameters of the studied induction heater.

Symbol	Quantity	Value
R	Workpiece thickness	80 mm
H	Workpiece height	200 mm
e	Air gap thickness between the load and the turns	20 mm
a	Width coil	15 mm
b	Distance between two slots	10 mm
h	Height of the first coil	100 mm
N	Number of turns	3
J	Current density	$3\,\mathrm{A/mm^2}$
f	Frequency	50
σ	Electrical conductivity	37.10^6 $(\Omega\mathrm{m}^{-1})$

The spatial distribution of the vector potential and magnitude of magnetic flux density along a radial and axial path are shown respectively in Figs. 4(a), 4(b) and Figs. 5(a), 5(b). We observe a growth of these quantities as a function of the radius and the height of the load up to maximum values at the points close to the coils.

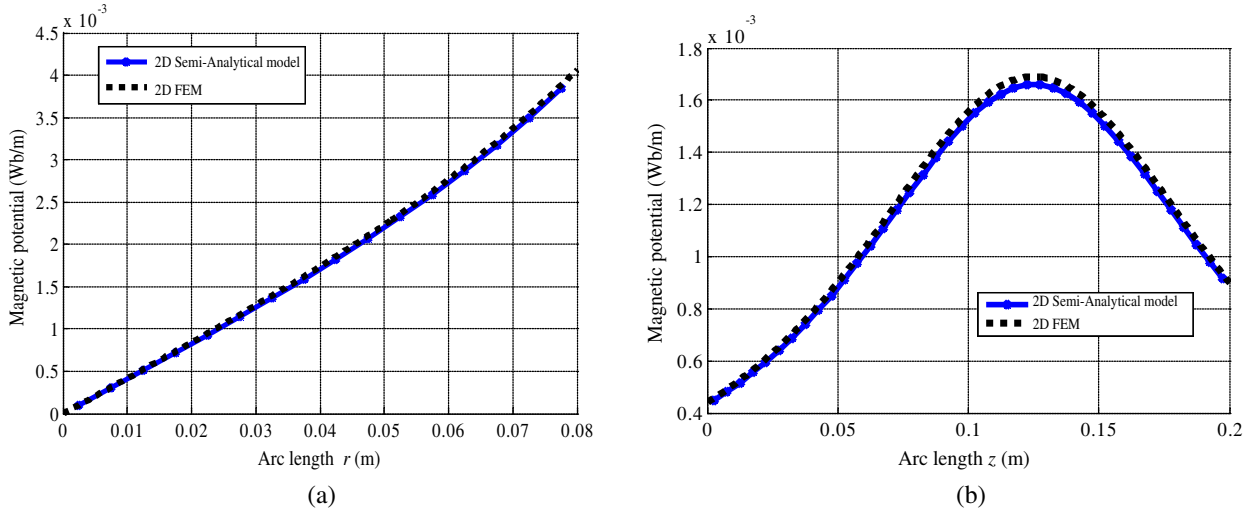

Figure 4. Magnetic Vector Potential: (a) versus the radial distance r (at $z = 0.01075\,\mathrm{m}$) for $f = 50\,\mathrm{Hz}$, versus the axial distance z (at $r = 0.0375\,\mathrm{m}$) for $f = 50\,\mathrm{Hz}$.

Using the semi-analytical model developed in 2D, the curves in Figs. 6(a) and 6(b) show the distribution of the radial component of the magnetic induction Br versus the radial distance r (at $z = 0.01075\,\mathrm{m}$) and versus the axial distance z (at $r = 0.0375\,\mathrm{m}$), respectively.

The eddy-current density and power density versus the radial distance r at $z = 0.1075\,\mathrm{m}$ are given in Fig. 7(a) and Fig. 7(b), respectively. Note that the values of the density of the induced currents in the room and consequently the power density are high in the areas closest to the inductor, and these densities decrease their minimum values near the axis of the cylinder and completely cancel the axis. All of these presented results obtained by semi-analytical model are also compared with those obtained by the 2D numerical model. We observe a very good agreement between these results.

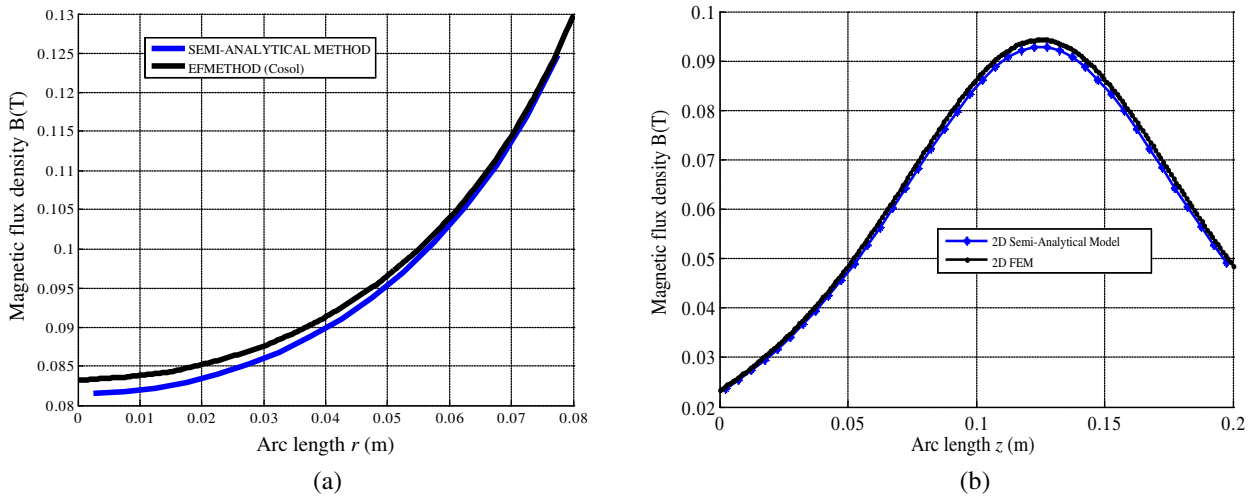

Figure 5. Magnetic flux density: (a) versus the radial distance r (at $z = 0.01075\,\mathrm{m}$) for $f = 50\,\mathrm{Hz}$, (b) versus the axial distance z (at $r = 0.0375\,\mathrm{m}$), $f = 50\,\mathrm{Hz}$.

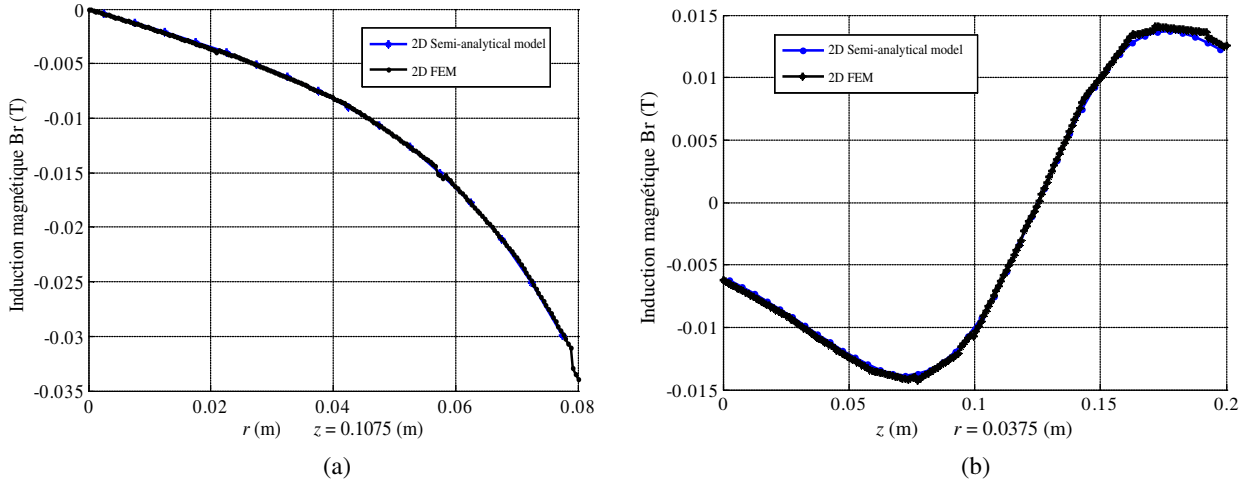

Figure 6. Magnetic flux density Br Component: (a) versus the radial distance r (at $z = 0.01075\,\mathrm{m}$) for $f = 50\,\mathrm{Hz}$, (b) versus the axial distance z (at $r = 0.0375\,\mathrm{m}$), $f = 50\,\mathrm{Hz}$.

3.2. Transient Thermal Study

The spatio-temporal distribution of the temperature inside the conductive part, subjected to a heat source, is governed by the following equation:

$$\rho c_p \left(\frac{\partial T}{\partial t} \right) = \lambda \Delta T + p \tag{19}$$

In this section, the transient thermal problem is limited to the billet to be heated and processed in 2D (plane r-z), using finite element calculation software; considering adiabatic boundary conditions on surfaces of the billet (Neumann condition, convective heat flux null), and knowing that the initial temperature is $T_0 = 25°\mathrm{C}$, $e = 8\,\mathrm{mm}$, $J = 6\,\mathrm{A/mm^2}$, $f = 50\,\mathrm{hz}$.

Noting that the heat source is the induced power calculated previously, and the physical characteristics of the cylindrical aluminium part are the same as those mentioned in [2, 14]. Noting that all the physical parameters of the piece $\lambda(T)$, $\rho(T)$, and $cp(T)$ are dependent on temperature, and the expressions and values of these parameters corresponding to the initial temperature are shown in [14].

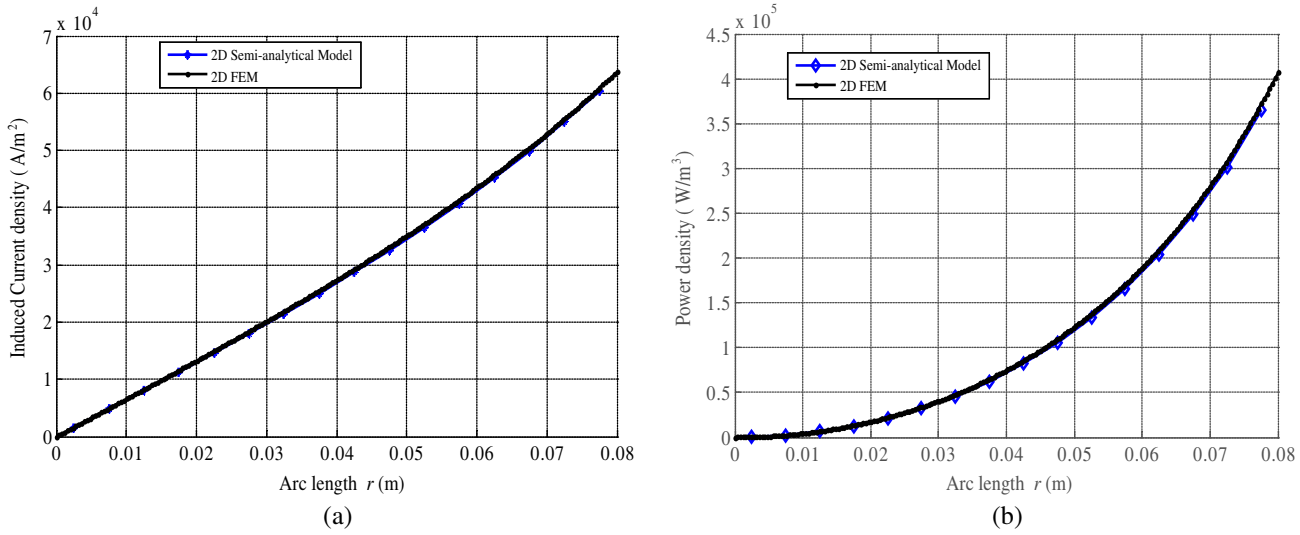

Figure 7. (a) Eddy-current density versus the radial distance r (at $z = 0.01075\,\mathrm{m}$) for $f = 50\,\mathrm{Hz}$. (b) Power density versus the radial distance r (at $z = 0.01075\,\mathrm{m}$) for $f = 50\,\mathrm{Hz}$.

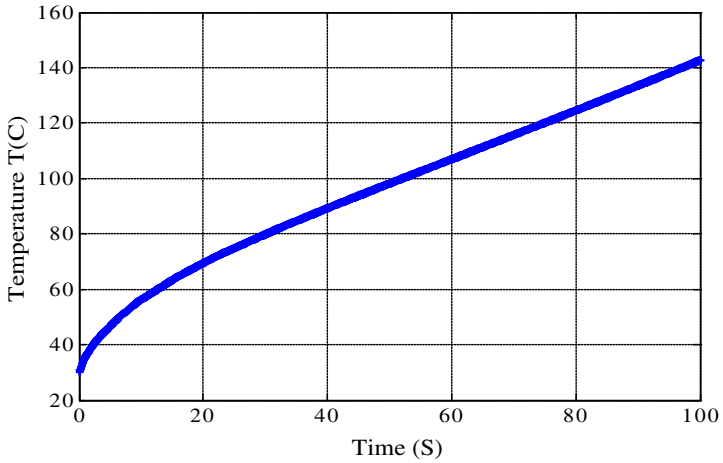

Figure 8. Temperature evolution at the surface of de workpiec ($z = 0.01075\,\mathrm{m}$, $r = 0.08\,\mathrm{m}$).

Figure 8 shows the evolution of the temperature over time at the surface of the part ($z = 0.01075\,\mathrm{m}$, $r = 0.08\,\mathrm{m}$). It can be seen that the temperature at the surface of the part is 140°C after 140 seconds of heating.

4. CONCLUSION

In this work, a quasi-2D analytical model is briefly presented. First, the analysis of the magnetic problem is performed based on the resolution of the electromagnetic equation by the elliptical integrals. Knowledge of the magnetic vector potential makes it easy to calculate other electromagnetic quantities such as magnetic induction, current density, and power dissipated by Joule.

Then to validate the semi-analytical model, we compared our results with those of the finite element method using the COMSOL Multiphysics software. We observed a good agreement between the two results. The proposed electromagnetic analytical model can be used as a quick and accurate design tool for heater devices.

REFERENCES

1. Rudnev, V., D. Loveless, R. Cook, and M. Black, *Handbook of Induction Heating*, Marcel Dekker, New York, 2003.
2. Abdi, A., Y. Ouazir, and G. Barakat, and Y. Amara, "Permanent magnet linear induction heating device: New topology enhancing performances," *COMPEL — The International Journal for Computation and Mathematics in Electrical and Electronic Engineering*, Vol. 37, No. 5, 1755–1767, Oct. 2018.
3. Ho, S. L., J. Wang, and Y. H. Wang, "A novel crossed traveling wave induction heating system and finite element analysis of eddy current and temperature distributions," *IEEE Transactions on Magnetics*, Vol. 45, No. 10, 4777–4780, Oct. 2009.
4. Ouazir, Y., A. Abdi, and H. Bensaidane, "2D analytical solution of transverse flux induction heating of the aluminum plates," *2012 XXth International Conference on Electrical Machines*, 2733–2738, Marseille, France, Sep. 2012.
5. Tavakoli, M. H., H. Karbaschi, and F. Samavat, "Computational modeling of induction heating process," *Progress In Electromagnetics Research Letters*, Vol. 11, 93–102, 2009.
6. Mach, F., P. Karban, I. Doležel, P. Šíma, and Z. Jelínek, "Model of induction heating of rotating non-magnetic billets and its experimental verification," *IEEE Transactions on Magnetics*, Vol. 50, No. 2, 309–312, Feb. 26, 2014.
7. Han, W., K. T. Chau, Z. Zhang, and C. Jiang, "Single-source multiple-coil homogeneous induction heating," *IEEE Transactions on Magnetics*, Vol. 53, No. 11, 1–6, Jun. 2017.
8. Moro1, F. and L. Codecasa, "A 3-D hybrid cell method for induction heating problems," *IEEE Transaction on Magnetics*, Vol. 53, No. 6, 1–4, Jun. 2017.
9. Qin, Z., H. Talleb, and Z. Ren, "A proper generalized decomposition-based solver for nonlinear magnetothermal problems," *IEEE Transactions on Magnetics*, Vol. 52, No. 1, 1–11, Oct. 2016.
10. D'Angelo, L. A. M. and H. De Gersem, "Quasi-3D finite-element method for simulating cylindrical induction-heating devices," *IEEE Transactions on Magnetics*, Vol. 2, 134–141, Aug. 2017.
11. Paul, S., J. Wright, and J. Z. Bird, "3-D steady-state eddy current dampingand stiffness for a finite thickness conductive plate," *IEEE Transactions on Magnetics*, Vol. 50, No. 11, 6301404, Nov. 2014.
12. Boughrara, K., F. Dubas, and R. Ibtiouen, "2-D exact analytical method for steady-state heat transfer prediction in rotating electrical machines," *IEEE Transactions on Magnetics*, Vol. 54, No. 9, 1–19, Sept. 2018.
13. Jin, P., Y. Tian, Y. Lu, Y. Guo, G. Lei, and J. Zhu, "3-D analytical magnetic field analysis of the eddy current coupling with Halbach magnets," *IEEE Transactions on Magnetics*, Vol. 56, No. 1, 1–4, Jan. 2020.
14. Abdi, A., Y. Ouazir, G. Barakat, and Y. Amara, "Transient quasi-3D magneto-thermal analytical solution in pm induction heating device," *COMPEL — The International Journal for Computation and Mathematics in Electrical and Electronic Engineering*, Vol. 39 No. 5, 1131–1144, 2020, https://doi.org/10.1108/COMPEL-01-2020-0054.
15. Lubin, T. and A. Rezzoug, "3-D analytical model for axial-flux eddy-current couplings and brakes under steady-state conditions," *IEEE Transactions on Magnetics*, Vol. 51, No. 10, 1–12, Oct. 2015.
16. Diriye, A., Y. Amara, and G. Barakat, "Three-dimensional modeling of permanents magnets synchronous machines using a 3D reluctance network," *2018 XIII International Conference on Electrical Machines*, 2304–2310, Alexandroupoli, Greece, Sep. 2018.
17. Jin, P., Y. Yuan, J. Minyi, F. Shuhua, L. Heyun, H. Yang, and S. L. Ho, "3-D analytical magnetic field analysis of axial flux permanent magnet machine," *IEEE Transactions on Magnetics*, Vol. 50, No. 11, 8103504, Nov. 2014.
18. Sahu, R., P. Pellerey, and K. Laskaris, "Eddy current loss model unifying the effects of reaction field and non-homogeneous 3-D magnetic field," *IEEE Transactions on Magnetics*, Vol. 56, No. 2, 1–4, Jan. 13, 2020.

19. Sun, X., S. Luo, L. Chen, R. Zhao, and Z. Yang, "Suspension force modeling and electromagnetic characteristics analysis of an interior bearingless permanent magnet synchronous motor," *Progress In Electromagnetics Research B*, Vol. 69, 31–45, 2016.
20. Verez, G., G. Barakat, and Y. Amara, "Influence of slots and rotor poles combinations on noise and vibrations of magnetic origins in 'U'-core flux-switching permanent magnet machines," *Progress In Electromagnetics Research B*, Vol. 61, 149–168, 2014.